PERGAMON

International Journal of Heat and Mass Transfer 44 (2001) 2461–2473

International Journal of HEAT and MASS TRANSFER

www.elsevier.com/locate/ijhmt

Classification and effects of thermal wakes on heat transfer in multilouvered fins

X. Zhang, D.K. Tafti *

National Center for Supercomputing Applications, 5600 Beckman Institute for Advanced Science and Technology, 405 North Mathews Avenue, Drawer 25, University of Illinois at Urbana-Champaign, Urbana, IL 61801, USA

Received 24 April 2000; received in revised form 28 August 2000

Abstract

The study classifies and isolates the effects of thermal wake interference that occurs in multilouvered fins. Inter-fin interference occurs between adjacent rows of louvers and is dominant at high flow efficiencies when the flow is louver directed. Intra-fin interference occurs on subsequent louvers of the same row or fin and is dominant at low flow efficiencies or when the flow is predominantly duct directed. It is established that thermal wake effects can be expressed quantitatively as functions of the flow efficiency and the fin pitch to louver pitch ratio. While the heat transfer capacity of multilouvered fins increases unconditionally when thermal wakes are eliminated, the heat transfer coefficient either increases or decreases depending on the relative location of thermal wakes in the vicinity of louvers. Experimental procedures, which neglect thermal wake effects in determining the heat transfer coefficient, while not introducing large errors at high flow efficiencies, can introduce errors as high as 100% at low flow efficiencies.

1. Introduction

Multilouvered fins find widespread use in the heating, ventilation and air-conditioning industries. Three important factors affect the heat transfer capacity in multilouvered geometries; they are the dominant flow direction, the presence of flow unsteadiness and associated large-scale structures, and thermal wake interference.

The importance of the predominant flow direction was recognized early in the design of multilouvers [1–3]. Two types of flow regimes were identified: louver directed flow, and duct directed flow. In the former, the predominant flow direction is aligned with the louvers, and in the latter the predominant flow direction is streamwise. This effect is quantified by defining a "flow efficiency", which is the ratio of the flow angle to the louver angle [3–5]. The heat transfer coefficient is affected favorably by louver directed flow. High Reynolds numbers, large louver angles, small fin pitches, thin louvers, and large louver pitches are conducive to louver directed flow.

Recently, Zhang et al. [6,7], Tafti et al. [8,9] have investigated the effect of self-sustained flow oscillations in the form of large-scale vorticity on the heat transfer coefficient. Tafti et al. [9] studied the transition from steady laminar to unsteady flow and its spatial propagation in a multilouvered fin array. The flow instability first appeared in the wake of the exit louver. Instabilities were then initiated in the downstream half of the array near the exit, which subsequently spread upstream into the multilouvered fin array as the Reynolds number increased. The onset of unsteadiness has a marked effect on the heat transfer coefficient, which increases due to the enhanced mixing provided by the large-scale vorticity in the vicinity of the louver surface. Large louver angles, high ratios of fin pitch to louver pitch, and thick louvers are conducive to the onset of unsteadiness. On the other hand, these same conditions can result in large recirculation zones at lower Reynolds numbers and decrease the heat transfer coefficient.

* Corresponding author. Tel.: +1-217-244-7385; fax: +1-217-244-2909.

E-mail address: dtafti@ncsa.uiuc.edu (D.K. Tafti).

0017-9310/01/$ - see front matter
PII: S0017-9310(00)00297-0

Nomenclature

b	fin thickness
F_p	non-dimensional fin pitch (F_p^*/L_p^*)
F_d	non-dimensional flow depth
k	thermal conductivity
L_p^*	dimensional louver pitch (characteristic length scale)
Nu^1	non-dimensional heat flux
Nu^2	non-dimensional heat transfer coefficient
Pr	Prandtl number
q	non-dimensional heat flux
Re_{in}	Reynolds number $(u_{in}^* L_p^*/v)$
S_1, S_2	non-dimensional entrance/exit and redirection louver dimensions
T	temperature
u, v	non-dimensional Cartesian velocity in x-, and y-direction, respectively
u_{in}^*	dimensional inlet velocity (characteristic velocity scale)

Greek symbols

α	flow angle
θ	louver angle
v	kinematic viscosity

Superscripts

$*$	dimensional quantities

Subscripts

f, fin	based on fin
in	based on inlet
louv	based on louver
out	based on outlet
mean	based on mixed mean
log	based on log mean

Although thermal wakes can be expected to have a very large effect on the heat transfer capacity of louvered fins, there has been no study devoted to this aspect. Our objective in this paper is to classify the thermal wakes and quantify their effects with the goal that a better understanding can lead to effective wake management techniques. This is done through numerical experiments, which are quite amenable to the manipulation of field quantities to simulate different scenarios.

The paper is organized as follows: First we give a brief description of the numerical procedure and the non-dimensional parameters used in characterizing heat transfer. This is followed by the classification of thermal wakes and the sensitivity of the heat transfer coefficient to their proximity to the louver surface. Then we selectively eliminate the different types of thermal wakes and quantify their effect on heat transfer. Finally, we use our results to estimate the experimental errors committed when thermal wake effects are neglected in determining the heat transfer coefficient.

2. Computational details

The governing equations for momentum and energy conservation are solved in a general boundary conforming coordinate system. They are discretized with a conservative finite-volume formulation. Both, convection and viscous terms are approximated by second-order central-difference schemes in a non-staggered arrangement. The computational unit, shown in Fig. 1(a) by the dotted lines, consists of one entire row of the louvered fin geometry allowing for the inclusion of entrance and exit effects in the flow direction. Periodic

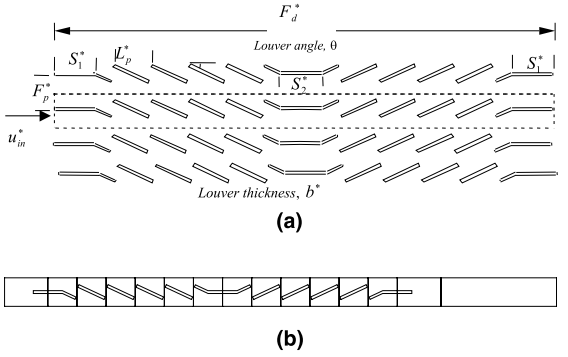

Fig. 1. (a) Cross-section of multilouvered fin array. Dotted lines show the basic computational unit; (b) multi-block domain decomposition.

boundary conditions are applied in the transverse direction, while Dirichlet boundary conditions are specified at the entrance to the array. The application of periodicity in the transverse direction allows the inclusion of thermal wake effects between successive rows of fins.

The governing equations are non-dimensionalized by a characteristic length given by the louver pitch L_p^*, a characteristic velocity scale given by the inlet velocity to the array (u_{in}^*) and a temperature scale given by $(T_f^* - T_{in}^*)$, where T_f^* is the specified fin surface temperature. The non-dimensionalization results in a characteristic Reynolds number $Re = Re_{in} = u_{in}^* L_p^*/v$, with Dirichlet boundary conditions $u_{in} = 1$, $T_{in} = 0$ at the entrance to the computational domain. The Prandtl number is fixed at 0.7 for air. At the fin surface, no slip, no penetration boundary conditions for the velocity

field, and $T_f = 1$ for the temperature field are applied. Due to the recovering nature of the flow at the array exit, convective outflow boundary conditions are applied at this boundary. Details about the time-integration algorithm, treatment of boundary and louver surface conditions, and validation of the computer program can be found in Tafti et al. [8,10].

The configuration used in these calculations consists of an entrance and exit louver with four louvers on either side of the center or redirection louver. For all the calculations in this paper the louver thickness is fixed at $b = 0.1$. For the entrance and exit louvers, $S_1 = 1$, and for the center redirection louver, $S_2 = 1$. Fig. 1(b) shows the computational domain which is resolved by 15 blocks, one for each louver, two each for the entrance, exit and redirection louver. The exit domain extends approximately 5.5 non-dimensional units (or 55 fin thicknesses) downstream of the array. Each block is resolved by 96×96 finite-volume cells (a total of 138,240 cells). A grid independency study was performed at a resolution of 128×128 cells in each block (a total of 245,760 cells). The time mean Nusselt number calculated on the 96×96 grid was within *one* percent of the fine grid calculation for $F_p = 1.5$ and $Re_{in} = 1000$. All results reported here are for 96×96 grid per block resolution. For the unsteady cases, time-averaged values are presented.

3. Characterization of heat transfer

We first define the relationship between dimensional and non-dimensional parameters used to quantify the heat transfer. The non-dimensionalization above results in two Nusselt numbers, one which is representative of the average non-dimensional heat flux, and the other of the non-dimensional heat transfer coefficient. The dimensional heat flux on the louver surface is defined as

$$q^* = -k\frac{\partial T^*}{\partial n^*} = h^*(T_f^* - T_{ref}^*), \tag{1}$$

where n^* is measured along the normal to the louver surface, and T_{ref}^* is a reference temperature. The above equation can also be expressed in terms of dimensional and non-dimensional parameters as

$$q^* = -\frac{k}{L_p^*}(T_f^* - T_{in}^*)\frac{\partial T}{\partial n} = h^*(1 - T_{ref})(T_f^* - T_{in}^*). \tag{2}$$

Rewriting Eq. (2) we can define the non-dimensional heat flux and Nusselt number as

$$Nu = \frac{h^* L_p^*}{k} = \frac{-\partial T/\partial n}{(1 - T_{ref})} \quad \text{and} \quad q = \frac{q^* L_p^*}{k(T_f^* - T_{in}^*)} = -\frac{\partial T}{\partial n}. \tag{3}$$

When $T_{ref} = T_{in} = 0$, we define a local Nusselt number on the louver surface as

$$Nu^1 = q = -\frac{\partial T}{\partial n}. \tag{4}$$

Further, an average Nusselt number on each louver

$$\langle Nu^1 \rangle_{louv} = \frac{\sum q \partial \Omega_{louv}}{\Omega_{louv}} = -\frac{\sum (\partial T/\partial n)\partial \Omega_{louv}}{\Omega_{louv}} \tag{5}$$

and for the whole multilouvered fin

$$\langle Nu^1 \rangle_{fin} = \frac{\sum q \partial \Omega_{fin}}{\Omega_{fin}} = -\frac{\sum (\partial T/\partial n)\partial \Omega_{fin}}{\Omega_{fin}} \tag{6}$$

can also be defined, where Ω denotes the heat transfer surface area. We note that for $T_{ref} = T_{in}$, the calculated Nusselt number is identical to the non-dimensional heat flux. Another Nusselt number based on a reference temperature

$$Nu^2 = \frac{h^* L_p^*}{k} = \frac{-\partial T/\partial n}{(1 - T_{ref})} \tag{7}$$

can also be defined, where T_{ref} can either be given by the mixed mean temperature

$$T_{ref} = T_{mean} = \frac{\sum_{F_p, L_p \text{ or } F_d} |u| T \, \Delta y \, \Delta x}{\sum_{F_p, L_p \text{ or } F_d} |u| \, \Delta y \, \Delta x} \tag{8}$$

or the log-mean temperature [1]

$$T_{ref} = T_{log} = 1 - \frac{T_{out} - T_{in}}{\ln\{(1 - T_{in})/(1 - T_{out})\}}. \tag{9}$$

Based on the above definition we define two additional Nusselt numbers, one for each individual louver, $\langle Nu^2 \rangle_{louv}$, and the other for the whole multilouvered fin, $\langle Nu^2 \rangle_{fin}$. For the former, T_{mean}, T_{out}, and T_{in} are calculated based on the computational block or blocks surrounding the louver, and in the latter they are calculated for the whole multilouvered fin (based on the flow depth F_d).

The definition of Nu^1 is not only a function of the geometry and the fluid mechanics, but also that of the temperature potential. Hence, although it is the single most important value in quantifying the heat transfer for a given louver geometry, because of its dependence on the temperature potential it cannot be used effectively to compare the performance of different louver geometries. For example, if we consider two identical geometries, except for one having more louvers than the other,

[1] The mixed mean temperature and log-mean temperature are identical for linear variations. In this study we use the mixed mean temperature as the reference temperature. The difference between the two is negligible when applied on a louver-by-louver basis. Across the whole fin, the difference increases when the variation of T_{ref} in the flow direction departs from a linear variation. This is often the case for low Reynolds numbers when the reference temperature saturates after the first few louvers.

because the average temperature potential is different in the two cases, so will Nu^1. On the other hand, the definition of Nu^2 based on a reference temperature, removes the average effect of the temperature potential. By removing the mean effect of the temperature potential on heat transfer, Nu^2 is representative of the heat transfer coefficient and is much more suitable for the comparative evaluation of different louver geometries. However, it is not an absolute quantity and has to be used with T_{ref} to obtain the heat transfer capacity of the fin. Our discussion in this paper will focus on both the heat flux and the heat transfer coefficient.

4. Classification of thermal wakes

Table 1 lists all the cases which are studied. Cases 1–5 have a fin pitch ratio of 1.0, whereas cases 6–8 have a fin pitch ratio of 1.5. Most of our discussion will focus on cases 1–5, which capture the essential elements of this study. The final results are summarized for all cases. The cases selected were primarily governed by the flow efficiency (η), which ranges from near complete louver directed flow to near complete duct directed flow. The flow efficiency is calculated as α_{avg}/θ, where α is the flow angle and θ is the louver angle. The flow angle for each louver is calculated based on $\alpha = \tan^{-1}(m_y/m_x)$, where $m_y = \int v\,dx$ and $m_x = \int u\,dy$ are the average mass flow rates calculated at the top and left face of the computational block surrounding each louver, respectively. An average value of α based on louvers 2–5 and 7–10 (the entrance, redirection, and exit louvers are not included) is used in calculating the flow efficiency for the fin. This procedure for calculating flow efficiency differs from experimental techniques, which usually use dye injection at the inlet to obtain the flow efficiency. For cases 1 and 2, the flow is primarily louver directed with very high flow efficiencies. Case 5 has the lowest flow efficiency for $F_p = 1.0$, whereas cases 3 and 4 exhibit intermediate flow efficiencies. The flow efficiencies for $F_p = 1.5$ range from 0.57 for case 6 to 0.14 for case 8. The flow efficiencies together with the geometrical information are listed in Table 1.

Fig. 2(a)–(d) plots the mean temperature contours for cases 1–4. Because of the periodicity in the transverse direction the calculations include the effects of thermal wakes. For cases 1 and 2 the temperature contours predominantly follow the louver direction, whereas for case 4 the predominant direction is the x- or streamwise direction.

Table 1
Summary of calculations performed

Case	F_p^*/L_p^*	Re_{in}	θ	η		$\langle Nu^1\rangle_{fin}$	T_{mean}	$\langle Nu^2\rangle_{fin}$
1	1.0	1000	30	0.94	With thermal wake effect	13.45	0.313	19.77
					No inter-fin wake effect	19.45	0.068	21.02
					No wake effect	19.91	0.042	20.91
2		1000	25	0.88	With thermal wake effect	14.53	0.348	22.19
					No inter-fin wake effect	18.68	0.085	20.5
					No wake effect	19.57	0.042	20.52
3		700	15	0.74	With thermal wake effect	11.37	0.414	19.34
					No inter-fin wake effect	14.18	0.181	17.24
					No wake effect	15.99	0.055	16.98
4		100	15	0.52	With thermal wake effect	2.45	0.672	7.65
					No inter-fin wake effect	3.83	0.341	5.72
					No wake effect	8.23	0.127	9.57
5		50	15	0.31	With thermal wake effect	1.26	0.78	6.31
					No inter-fin wake effect	2.76	0.375	4.38
					No wake effect	7.29	0.154	8.79
6	1.5	500	30	0.57	With thermal wake effect	9.96	0.348	14.79
					No inter-fin wake effect	12.62	0.105	14.21
					No wake effect	13.24	0.039	13.84
7		200	15	0.38	With thermal wake effect	4.08	0.377	6.57
					No inter-fin wake effect	4.35	0.25	5.88
					No wake effect	9.06	0.051	9.61
8		50	15	0.14	With thermal wake effect	1.56	0.545	3.48
					No inter-fin wake effect	1.87	0.343	2.88
					No wake effect	6.92	0.092	7.69

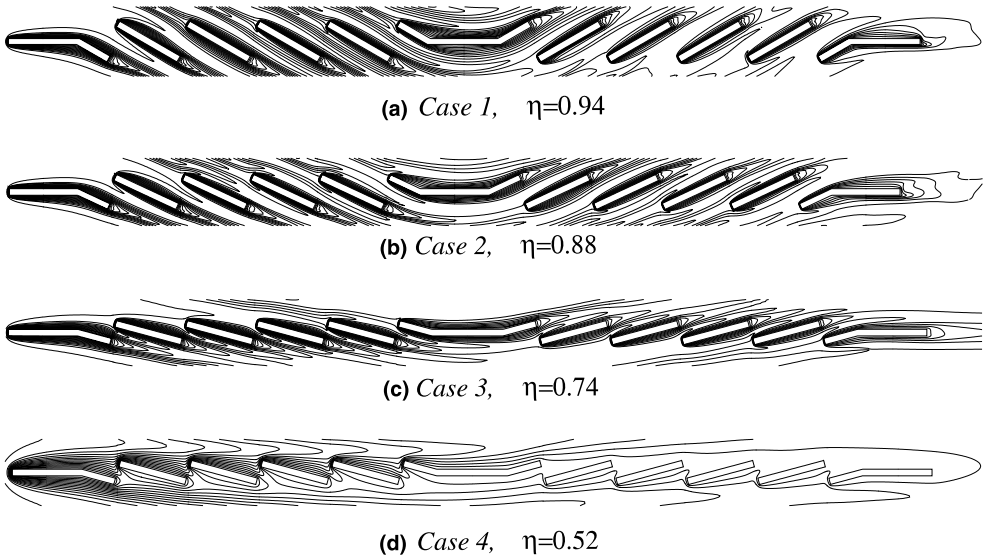

Fig. 2. Mean temperature contours with thermal wake effects.

From Fig. 2, we classify two primary mechanisms by which thermal wakes interfere with downstream louvers.

(a) Intra-fin interference. In this mode of interference, wakes of upstream louvers interfere with louvers downstream in the same fin. There are two types of intra-fin interference. The first type is dominant in duct directed flow, in which the thermal wakes of upstream louvers interfere with successive downstream louvers. This type of interference is dominant at low flow efficiencies as seen in Fig. 2(d). The second type can be more clearly identified in louver directed flow at higher flow efficiencies (however, it is also present in duct directed flow), in which the wakes of upstream louvers impinge on louvers downstream of the re-direction louver in the same fin row. We consider this as having a secondary effect, since the thermal wake is considerably diluted and weakened by the time it interferes with any louver. This type of interference is present for large fin pitches, and small louver angles.

(b) Inter-fin interference. Inter fin interference is present in both duct directed and louver directed flows, although it is best illustrated in louver directed flow, when thermal wakes between fin rows interfere with each other. In louver directed flow this is the dominant form of wake interference and is quite well illustrated in Fig. 2(a) for 30°. Suga and Aoki [11] assuming a linear wake trajectory, and 100% flow efficiency, gave the following expression for estimating thermal wake effects.

$$\frac{F_{\mathrm{p}}^{*}}{L_{\mathrm{p}}^{*}\tan(\theta)} = n. \tag{10}$$

Values of n close to an integer value $(2, 3, \ldots)$ signal wake interference, whereas values of $(1.5, 2.5 \ldots)$ indicate little or no interference. The interference gets weaker as the value of n increases. We have found that using the actual flow angle (α) instead of the louver angle gives much better prediction accuracy. For example, for cases 1 and 2, the calculated average flow angles are 28.2° and 22°, respectively. Using these values the predictions are much more in agreement with what is observed in Fig. 2(a) and (b). For the 30° louvers $(n = 1.88)$, there is much greater thermal wake interference than for the 25° louvers $(n = 2.48)$.

Fig. 3(a) plots variations in $\langle Nu^{1}\rangle_{\mathrm{louv}}$ or non-dimensional heat flux on a louver-by-louver basis. For predominantly duct directed flow (cases 4 and 5) there is a sharp drop in the heat flux immediately after the entrance louver. The flux decreases further in the first five louvers and only a small fraction of the total heat transferred is from louvers downstream of the re-direction louver. This is a result of the low Reynolds number (low mass flow rate), and the duct flow regime. The former induces thermal saturation, whereas the latter encourages high intra-fin thermal wake interference. At higher Reynolds numbers and larger flow angles, the flow is louver directed. Hence, for cases 1 and 2, the drop in heat flux is not monotonic and not as dramatic but more gradual. The non-monotonicity is primarily caused by the presence or absence of thermal wakes in the vicinity of louver surfaces. It is interesting to note that a difference of 5° in the louver angle (between cases 1 and 2) has a significant effect on the heat flux distribution. The average heat flux for the whole fin or $\langle Nu^{1}\rangle_{\mathrm{fin}}$ is listed in Table 1 for each case.

Fig. 3(b) plots the distribution of T_{mean} on a louver-by-louver basis for the three cases. The effective T_{mean} for

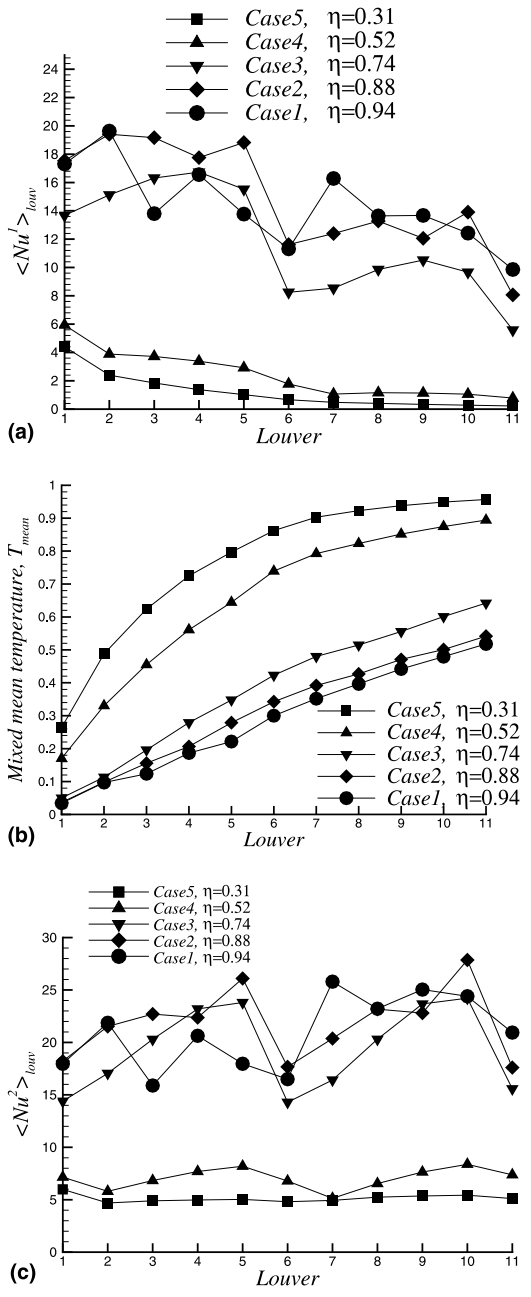

Fig. 3. (a) Louver-by-louver distribution of average heat flux; (b) variation of mixed mean temperature; (c) louver-by-louver distribution of heat transfer coefficient.

the whole fin is listed in Table 1. The distribution of T_{mean} is dependent on the heat transferred from upstream louvers. For cases 1 and 2, T_{mean} increases linearly into the array and reaches a value near 0.5 at the exit louver. On the other hand, for cases 4 and 5, T_{mean} increases rapidly in the first half of the array and then increases gradually thereafter to a near asymptotic value at the exit louver.

5. Sensitivity of the heat transfer coefficient to thermal wakes

In this section, the sensitivity of the heat transfer coefficient or Nu^2 to the mixed mean temperature is illustrated. We compare two cases, one in which the heat flux or $\langle Nu^1\rangle_{\text{louv}}$ and T_{mean} are different but the resulting heat transfer coefficient or $\langle Nu^2\rangle_{\text{louv}}$ is the same. In the second case, we study a situation in which the heat fluxes are nearly the same but the resulting heat transfer coefficients are different.

To first-order the heat transfer coefficient is a function of the hydrodynamic field surrounding each louver. For example, a louver experiencing unsteady flow oscillations in the vicinity of its surface will in general exhibit a higher heat transfer coefficient than its counterpart with steady laminar flow. Louvers 4 and 9 in case 4 exhibit different heat fluxes and different mixed mean temperatures (see Fig. 3(a) and (b)). However, the hydrodynamics in the vicinity of both louvers is similar and the application of Eq. (7) eliminates the difference in temperature potential and results in the same heat transfer coefficient (see Fig. 3(c)). This is also reflected in the normalized temperature contours plotted in Fig. 4(a) and (b) as $(T - T_{\text{mean}})/(1 - T_{\text{mean}})$, which exhibit very similar distributions and gradients in the vicinity of the louver. Here T_{mean} is calculated based on the fluid surrounding the louver.

The heat transfer coefficient is also sensitive to the location of thermal wakes. For louvers with the same hydrodynamics and the same heat fluxes, the calculated heat transfer coefficient is dependent on the location of thermal wakes with respect to the louver surface. To illustrate this effect we use louvers 4 and 5 from case 2. The flow field for the two louvers is very similar with recirculation zones in the leading edge region of the top surface. However, thermal wakes from upstream louvers are in closer proximity to the bottom surface of louver 4 than in louver 5, where instead cold free-stream fluid passes in the vicinity. From Fig. 3(a), the heat flux on louver 5 is larger than louver 4 by 6%. However, the calculated heat transfer coefficient is 18% higher (see Fig. 3(c)). Contours of $(T - T_{\text{mean}})/(1 - T_{\text{mean}})$ in Fig. 4(c) and (d) show the higher temperature gradients in the vicinity of the bottom surface of louver 5.

Hence, the heat transfer coefficient is not only sensitive to the hydrodynamics of the flow field around the louver but also to the presence or absence of thermal wakes in the vicinity of the louver surface. Fig. 3(c) plots the mean heat transfer coefficients on a louver-by-louver basis for cases 1–5. For cases 4 and 5, the hydrodynamic field and thermal wake effects are quite

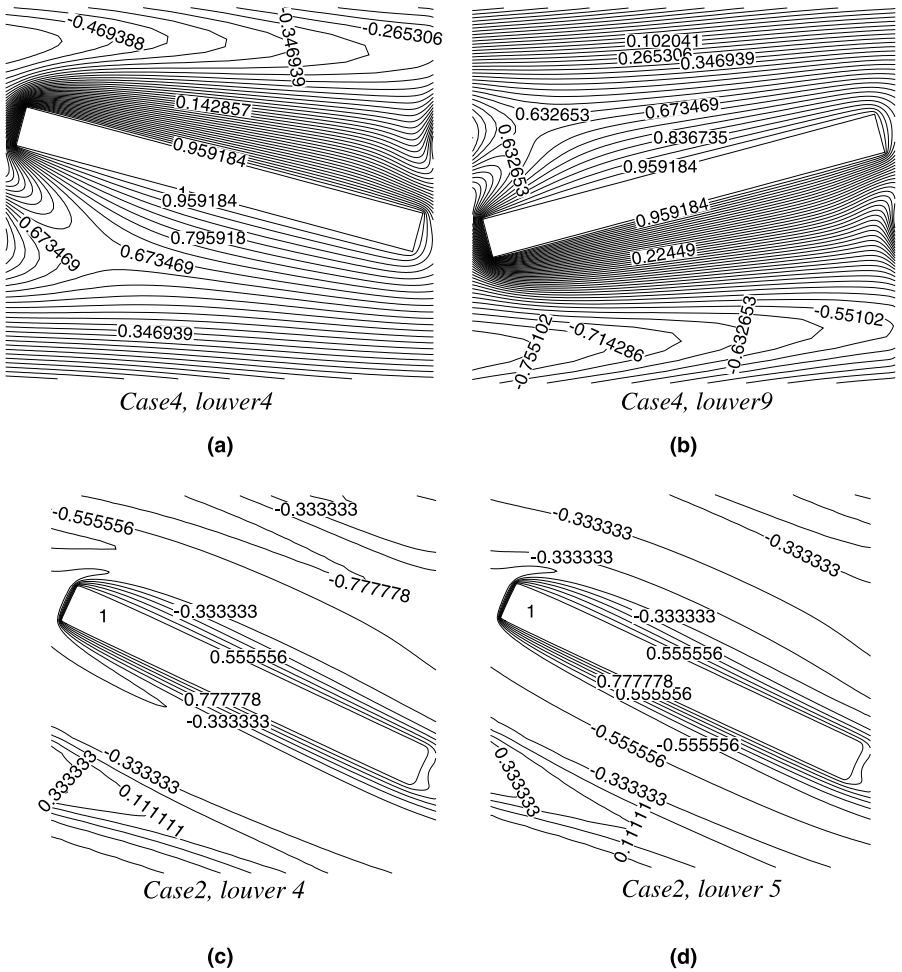

Fig. 4. Comparison of $(T - T_{\text{mean}})/(1 - T_{\text{mean}})$ surrounding different louvers to establish effect of hydrodynamics and thermal wakes on louver heat transfer coefficient.

uniform and homogeneous around each louver, and hence the heat transfer coefficients are quite symmetrical about the redirection louver, in spite of large differences in the heat flux. Louvers 5 and 10 in case 2, exhibit very high heat transfer coefficients. This primarily results from the inhomogeneity in the thermal field surrounding the louvers. Cold free-stream fluid flows in the vicinity of the louvers, increasing the heat flux. At the same time the presence of thermal wakes away from the louver results in high values of T_{mean}. These effects combine to produce high heat transfer coefficients. Conversely, in case 1, louvers 3 and 8 exhibit low heat transfer coefficients because of the presence of thermal wakes in the vicinity of the louvers. Also unsteady flow oscillations and vortex shedding in the downstream half of the array, cause the mean heat transfer coefficients to be higher in the downstream half of the fin array in case 1.

The mean heat transfer coefficient, $\langle Nu^2 \rangle_{\text{fin}}$ for the fin is listed in Table 1 for all cases. It is found that in spite of the higher flow efficiency exhibited by case 1, case 2 has the higher heat transfer coefficient. This is a result of less inter-fin thermal wake interference in case 2.

6. Quantification of thermal wake effects on heat flux and heat transfer coefficient

In this section we evaluate the effect of the intra- and inter-fin thermal wakes on heat flux and the heat transfer coefficient. In order to isolate these effects, two additional numerical experiments are performed for each case. In the first, the inter-fin wake is eliminated. This is done by artificially setting the temperature to the free-stream temperature $(T = 0)$ for any fluid leaving the calculation domain at the top and bottom boundaries of

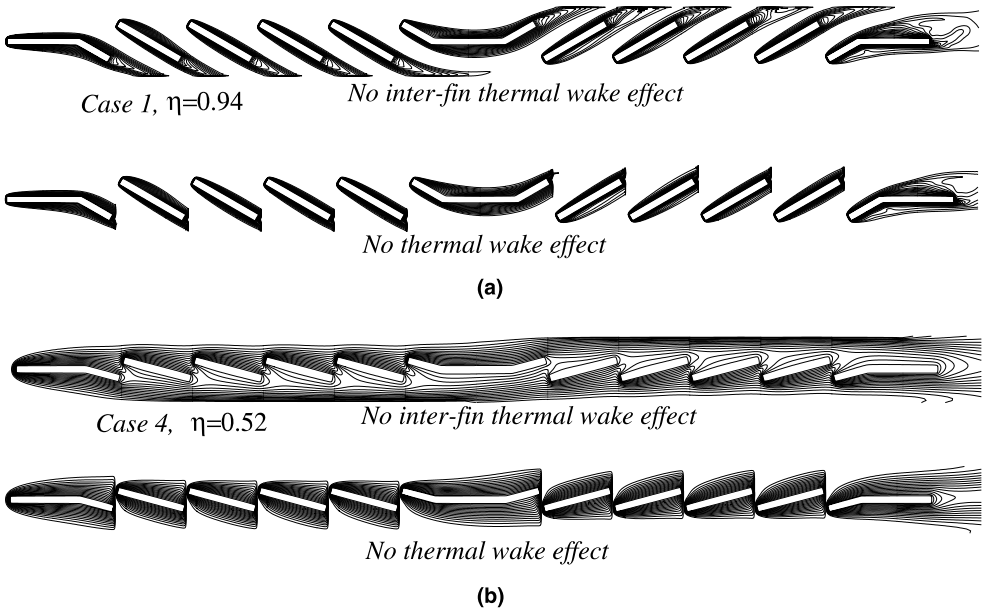

Fig. 5. Temperature contours on removal of inter-fin and intra-fin thermal wakes.

the calculation domain. Admittedly by doing this, we also eliminate part of the intra-fin wake, in which louver wakes upstream of the redirection louver impinge on downstream louvers of the same fin. However, as stated earlier this type of interference is secondary and will have a marginal effect. To a very good approximation, these experiments isolate the effect of inter-fin thermal wakes on heat flux and the heat transfer coefficient.

In the second set of experiments, the intra-fin wake is eliminated by setting the temperature to zero for fluid leaving the streamwise block boundary downstream of each louver [2]. Hence, in these set of runs all thermal wake effects are eliminated, and they represent the maximum possible or idealized heat flux for the given geometry and flow conditions.

Fig. 5(a) and (b) characterizes the elimination of the inter-fin and intra-fin wake for cases 1 and 4, which represent the two extremes of louver and duct directed flows. On comparison with Fig. 2, elimination of the inter-fin wake has a large effect on the temperature distribution for case 1, whereas it does not have such a dominant effect on case 4. On the other hand, further removal of the intra-fin wake has a negligible effect on case 1 but a much larger effect on case 4.

Fig. 6(a)–(d) compares the louver-by-louver distribution of $\langle Nu^1 \rangle_{\text{louv}}$ or heat flux for cases 1 to 4. For all cases the effect of thermal wakes is much stronger in the downstream half of the array as evidenced by the large increase in heat flux [3]. On elimination of thermal wakes, the heat flux is much more representative of the hydrodynamics. For example, cases 3 and 4 exhibit the same trends and numerical values on either side of the redirection louver, whereas case 1 exhibits higher values in the downstream half because of the flow unsteadiness. Removal of the inter-fin wake has a much larger effect on cases 1 and 2, whereas removal of the intra-fin wake has a larger effect on case 4. Both wakes have an equal effect on case 3.

The results for the fin are summarized for all cases in Table 1. Fig. 7(a) plots the percentage change in heat flux as the inter-fin wake and intra-fin wake are successively eliminated. Early on in this study, it was deduced that the effects pertaining to louver angle, fin pitch, and flow conditions could be lumped together in the flow efficiency to provide a single parameter to quantify the trends in the effect of thermal wakes on heat transfer. However, as we proceeded with the study, it was found that differences in fin pitch could not be reconciled by lumping its effect in the flow efficiency. We will expand more on this aspect later in the section. For now, we plot the results against the flow efficiency separately for the two fin pitch ratios. Both, inter- and

[2] In a numerical framework the order of wake elimination is important. A little reflection will show that eliminating the intra-fin wake first would also eliminate a large part of the inter-fin wake.

[3] Because of the numerical removal of the intra-fin wake, the heat flux increases near the trailing edge of the entrance louver. The increase is highest for case 5 and decreases rapidly for the other cases.

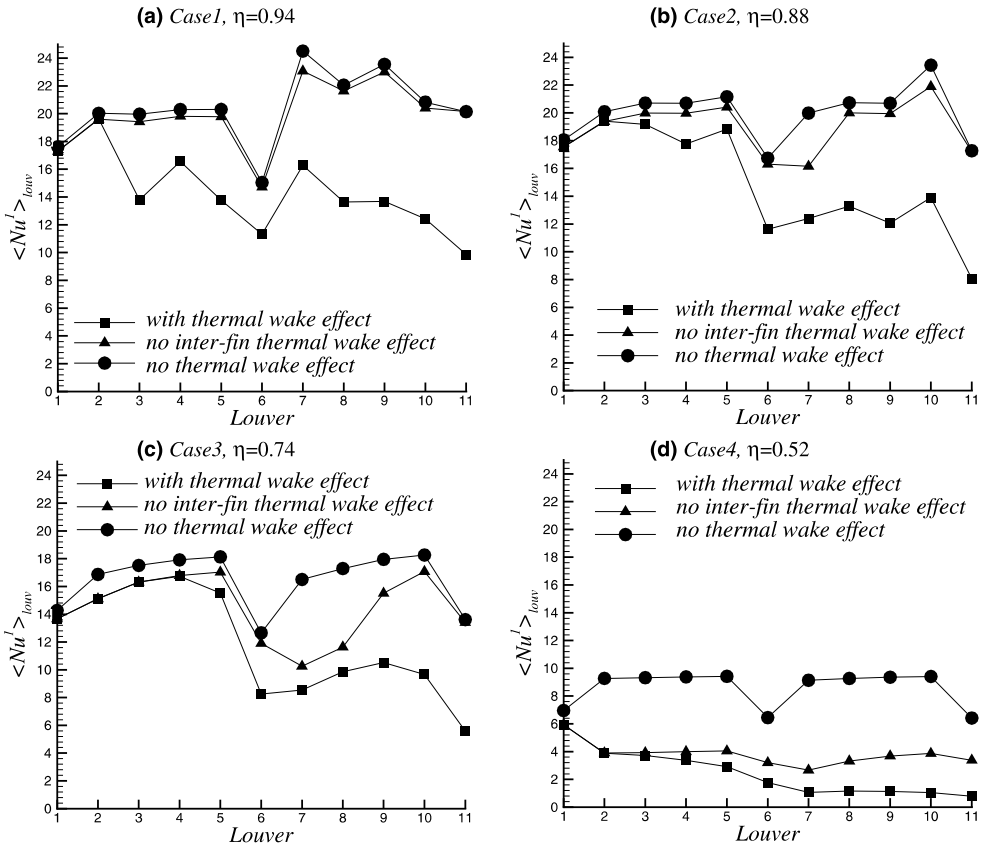

Fig. 6. Louver-by-louver distribution of average heat flux on removal of inter-fin and intra-fin thermal wakes.

intra-fin thermal wakes have a smaller effect on the heat transfer capacity of the fin for the larger fin pitch ratio. Overall, the increase in heat flux ranges from 50% at high flow efficiencies to nearly 500% for low flow efficiencies. Hence it is clear that for high heat capacity fins, the flow efficiency has to be made as high as possible to approach the maximum possible heat transfer. The values plotted in Fig. 7(a) are a function of the number of louvers or flow depth, hence are not absolute. A much better representation of the effect of thermal wakes on the heat transfer capacity is given by plotting the fraction

$$\phi = \frac{\langle Nu^1 \rangle_{\text{fin, no inter fin thermal wake}} - \langle Nu^1 \rangle_{\text{fin, with thermal wake}}}{\langle Nu^1 \rangle_{\text{fin, no thermal wake}} - \langle Nu^1 \rangle_{\text{fin, with thermal wake}}} \tag{11}$$

which defines the fractional increase in heat flux when the inter-fin wake is eliminated. The fraction $1-\phi$ characterizes the fractional increase on elimination of the intra-fin wake. This is plotted in Fig. 7(b). At low flow efficiencies, the inter-fin thermal wake has a small effect on the heat transfer capacity of the fin, whereas the intra-fin wake has a large effect. The trends are gradually reversed as the flow efficiency increases; at high flow efficiencies the inter-fin wake is nearly completely responsible for the reduction in heat capacity. For $F_p = 1.5$, the effect of inter-fin wake is weaker at low flow efficiencies, but increases rapidly as the flow efficiency increases to 0.57. Beyond $\eta > 0.45$, the inter-fin thermal wake has a larger effect on the fractional increase in heat flux for $F_p = 1.5$ than for $F_p = 1.0$, which is contrary to the general expectation.

By progressively eliminating thermal wake effects, the heat flux or Nu^1 increases, whereas T_{mean} decreases. Depending on the magnitude of the changes in these two quantities, the heat transfer coefficient or Nu^2 can either increase, decrease or remain the same. Consider Eq. (7) written in a modified form as:

$$Nu^2_{\text{nowake}} = \frac{h^* L^*_p}{k} = \frac{Nu^1_{\text{wake}} + \Delta Nu^1}{1 - \left(T_{\text{mean}_{\text{wake}}} - \Delta T_{\text{mean}}\right)}, \tag{12}$$

where ΔNu^1 and ΔT_{mean} are positive quantities and represent the increase in heat flux, and decrease in mixed mean temperature, respectively, when thermal wake effects are eliminated. Subtracting Eq. (12) from Nu^2_{wake} and some algebraic manipulation lead to the following three conditions:

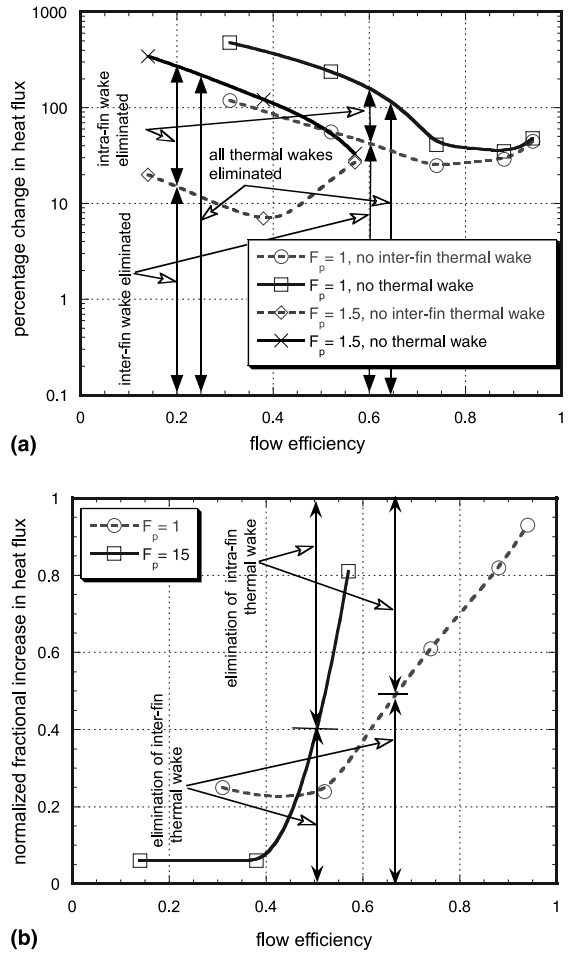

Fig. 7. Change in heat flux on removal of inter- and intra-fin wakes: (a) percentage change; (b) normalized fractional change.

$$\text{If } \Delta Nu^1/\Delta T_{\text{mean}} < Nu^2_{\text{wake}}, \quad \text{then } Nu^2_{\text{wake}} > Nu^2_{\text{nowake}}, \tag{13a}$$

$$\text{If } \Delta Nu^1/\Delta T_{\text{mean}} > Nu^2_{\text{wake}}, \quad \text{then } Nu^2_{\text{wake}} < Nu^2_{\text{nowake}}, \tag{13b}$$

$$\text{If } \Delta Nu^1/\Delta T_{\text{mean}} = Nu^2_{\text{wake}}, \quad \text{then } Nu^2_{\text{wake}} = Nu^2_{\text{nowake}}. \tag{13c}$$

The last condition for the equality of the two heat transfer coefficients states that on the removal of thermal wake effects the increase in heat flux should be proportional to the decrease in mixed mean temperature, with the proportionality constant given by the heat transfer coefficient. Physically, this condition can only be realized when the temperature field surrounding the louver is uniform with no spatial variations with and without thermal wakes. In reality though, this is never realized because the presence or absence of thermal wakes leads to spatial variations or inhomogeneities in the temperature field.

The first and second conditions can be directly related to the inhomogeneity of the temperature field by considering two limiting cases. The first condition (Eq. (13a)) physically represents the case when the thermal wake is strong but the trajectory is between louvers and does not influence the heat transfer at the surface. As a result when the wake is eliminated, the reduction in the mixed mean temperature is disproportionately larger than the increase in the heat flux. Hence the heat transfer coefficient decreases in the absence of the thermal wake. The second limiting condition (Eq. (13b)) occurs at the other extreme – when the thermal wake engulfs a louver, on its removal the increase in the heat flux is disproportionately larger than the reduction in the mixed mean temperature. In such instances, the heat transfer coefficient increases when the thermal wake effect is removed.

Fig. 8(a)–(d) compares the calculated heat transfer coefficients on a louver-by-louver basis in the presence of thermal wake effects, on the removal of the inter-fin wake (only intra-fin wake effects) and finally on the removal of the intra-fin wake effects (no thermal wakes). We note that louvers 5 and 10 in case 2, exhibit a decrease in heat transfer coefficients when the thermal wakes are removed. Going back to our discussion pertaining to Fig. 4(d), the scenario for these two louvers adheres to Eq. (13a). On the other hand, louver 3 in case 1, which is engulfed in the thermal wake of louver 1, exhibits an increase in the heat transfer coefficient on the removal of thermal wakes as per the condition in Eq. (13b).

Table 1 summarizes these results for the fin. Fig. 9 plots the percentage change in the heat transfer coefficient as the inter- and intra-fin wakes are successively eliminated. Thermal wake effects on the heat transfer coefficient are minimal at high flow efficiencies (within $\pm 15\%$), but increase as the flow efficiency decreases. Eliminating the inter-fin thermal wake reduces the heat transfer coefficient (within -30%), and the effect is much larger for the smaller fin pitch. When both the inter- and intra-fin wakes are eliminated, the heat transfer coefficient increases. The increase is quite rapid for the larger fin pitch (+120% at $\eta = 0.14$), while more gradual for $F_{\text{p}} = 1.0$.

It is interesting to note that "high" flow efficiency is relative for the two fin pitches. Even though the flow efficiency is only 0.57 for $F_{\text{p}} = 1.5$, the behavior exhibited in Figs. 7 and 9 is the same as that exhibited at a flow efficiency of 0.94 for $F_{\text{p}} = 1.0$. Our calculations for $\theta = 15, 20, 25$ and 30° louver angles for the two fin pitches show that for $F_{\text{p}} = 1.5$, the flow efficiencies asymptote to a value near 0.6 in the vicinity of $Re_{\text{in}} = 1200$, whereas for $F_{\text{p}} = 1.0$, the asymptotic values are much higher, near 0.98. Hence a better representation of

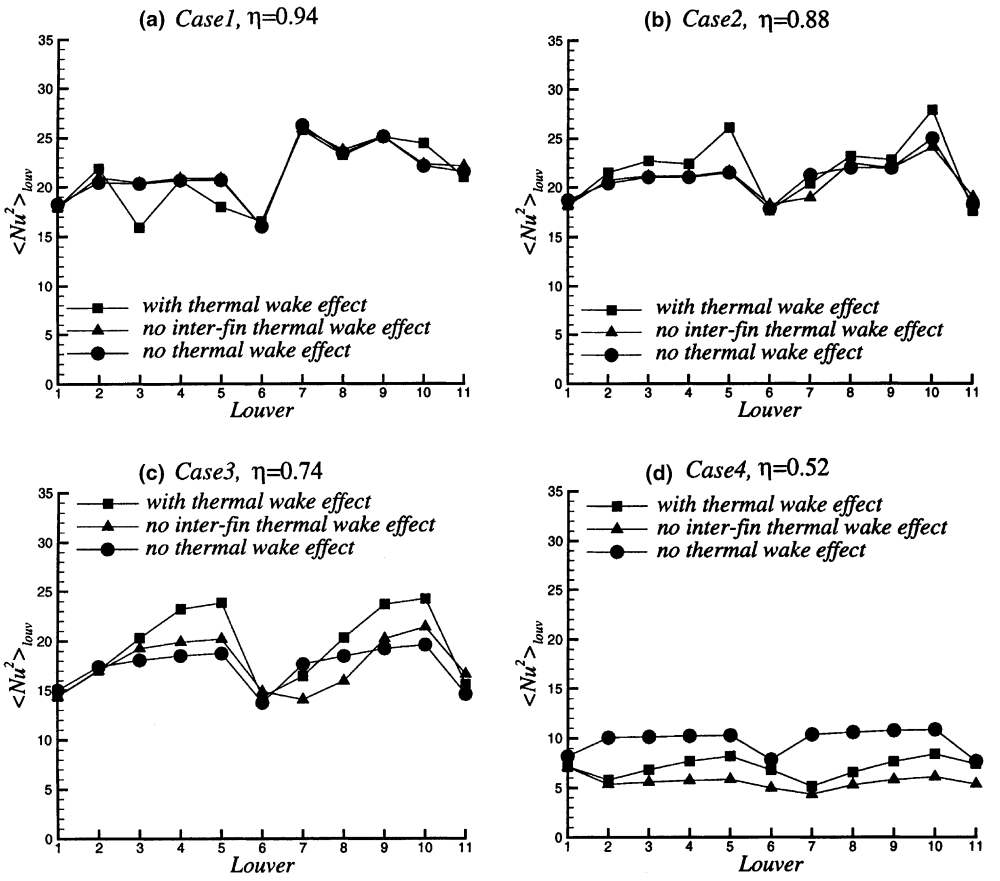

Fig. 8. Louver-by-louver distribution of average heat transfer coefficient on removal of inter-fin and intra-fin thermal wakes.

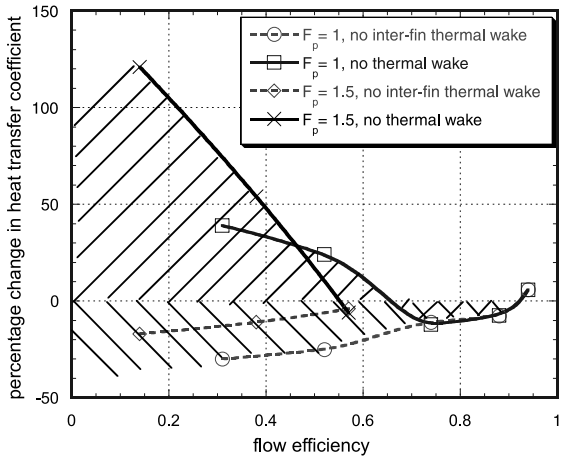

Fig. 9. Percentage change in heat transfer coefficient on removal of inter- and intra-fin wakes.

Figs. 7 and 9 would be to normalize the flow efficiencies by their asymptotic values for the two fin pitches. The curves for $F_p = 1.0$ will remain nearly the same, whereas those for $F_p = 1.5$ will be shifted to the right (the normalized values will be 0.95, 0.63, 0.23 for cases 6, 7 and 8, respectively). However, this procedure still does not completely reconcile the distinct difference between the two fin pitches. Hence, it can be concluded that flow efficiency is not a sole indicator of thermal wake effects; it has to be used with the fin pitch to louver pitch ratio.

7. Relationship of numerical experiments to laboratory experimental studies

In experimental investigations of louvered fin heat exchangers, there are two general approaches used. Investigations at the system level, in which heat exchanger cores are studied, use either the LMTD method [12] or the ε-NTU method [13,14] for deducing the heat transfer coefficient. These methods, though extremely useful in analyzing full system level performance, do not provide any insight into the fundamental mechanisms of fluid flow and heat transfer occurring in the heat exchanger. The other approach, more fundamental in nature, models multiple rows of louvered fins by either using a

Table 2
Actual and measured heat transfer coefficients when thermal wake effects are neglected

Case	Actual heat transfer coeff. $\langle Nu^2 \rangle_{fin}$	Measured heat transfer coefficient with one row heated	Measured heat transfer coefficient with one louver heated
1	19.77	19.45	19.91
2	22.19	18.68	19.57
3	19.34	14.18	15.99
4	7.65	3.83	8.29
5	6.31	2.76	7.29
6	14.79	12.62	13.24
7	6.57	4.35	9.06
8	3.48	1.87	6.92

mass transfer analogy [15] or by heating the louvers [16]. The multiple rows provide the same hydrodynamic effect as an infinite array of louvers encountered in real heat exchangers. However, in most instances, either a single fin (or 1 row) in the array, or in some instances only single louvers are coated with naphthalene or heated to obtain the mass or heat transfer coefficient. Further, the mass/heat transfer coefficient is obtained by assuming a zero mean concentration of naphthalene in the vicinity of the fin or the louver [4]. This procedure implicitly assumes that thermal wake effects on mass/heat transfer coefficient are minimal and can be neglected. We examine these assumptions by using the results of our numerical experiments.

In the numerical experiments, the case in which the inter-fin wake is eliminated corresponds to the experimental scenario in which only a single row provides an active heat or mass transfer surface. This row does not feel the effects of thermal or mass wakes from any other fin, but only feels the effect of its own (intra-fin) thermal/mass wake. On the other hand, the numerical case in which all wake effects are eliminated corresponds to the experimental case in which only a single louver provides an active heat/mass transfer surface. This louver does not feel any thermal wake effects. Further, in both experimental scenarios, by assuming that the reference temperature is the same as the inlet temperature (mass concentration of zero), what is being measured as the heat transfer coefficient is in actuality the heat flux or Nu^1.

Table 2 examines the two cases; when a single row of louvers provides the active heat/mass transfer surface, and when one louver provides the active heat/mass transfer surface. The second column shows the actual calculated heat transfer coefficient $\langle Nu^2 \rangle_{fin}$ with all thermal wake effects included. The third column is the measured experimental heat transfer coefficient with one row heated, which in actuality is $\langle Nu^1 \rangle_{fin}$ with the inter-fin thermal wake eliminated. For the scenario in which a single louver provides the active heat/mass transfer surface, experiments measure the heat flux or $\langle Nu^1 \rangle_{fin}$ with no thermal/mass wake effects as the heat transfer coefficient. This is shown in column 4 [5].

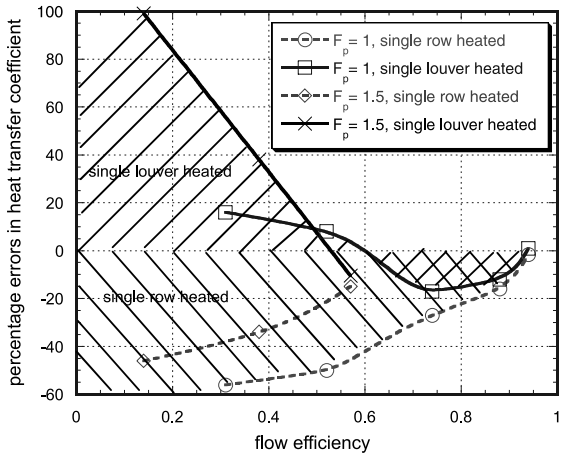

Fig. 10. Percentage errors in experimentally determined heat transfer coefficients when thermal wake effects are neglected.

Fig. 10 summarizes the resulting errors that occur when using these procedures. When a single row provides the active heat/mass transfer surface, the measured heat transfer coefficient is underpredicted. The underprediction ranges from <20% for high flow efficiencies (>0.8 for $F_p = 1.0$, >0.5 for $F_p = 1.5$) to about 50% at low flow efficiencies. The errors are less severe for the larger fin pitch. For the case in which a single louver provides the heat/mass transfer surface, the resulting measurements overpredict the heat transfer coefficient except in the high range of flow efficiencies where it is underpredicted (within −20%). The overprediction is much larger for the larger fin pitch ratio (up to 100% at low flow efficiencies), whereas less severe (<20%) for the

[4] In the case of heat transfer experiments, the inlet temperature is used to obtain the heat transfer coefficient.

[5] In presenting this result it is assumed that experimentally the average heat transfer coefficient for the whole fin is obtained by averaging the measured heat transfer coefficient for each louver weighted by the area of each louver.

smaller fin pitch. These results also indicate, quite contrary to expectations, that using single louvers (versus a row) as the active surface provides a better approximation to the actual heat transfer coefficient for the larger fin pitch. Whereas, for the smaller fin pitch, a full row as the active surface provides the better approximation.

8. Conclusions

The study classifies two types of thermal wake interferences that occur in multilouvered fins. Inter-fin interference occurs between adjacent rows of louvers and is dominant at high flow efficiencies when the flow is louver directed. Intra-fin interference occurs on subsequent louvers of the same row or fin and is dominant at low flow efficiencies or when the flow is predominantly duct directed. It is shown that thermal wake effects can be expressed as functions of the flow efficiency and the fin pitch-to-louver pitch ratio.

While the heat transfer capacity of multilouvered fins increases unconditionally when thermal wakes are eliminated, the heat transfer coefficient either increases or decreases depending on the location of thermal wakes in the vicinity of the louver. The increase in heat flux or heat transfer capacity is larger for small pitch ratios. On the other hand, the heat transfer coefficient decreases on elimination of the inter-fin thermal wake and increases with the elimination of all thermal wakes. The increase is much larger as the fin pitch increases.

Finally, we relate the numerical calculations to experimental studies which neglect the effect of thermal wakes in determining the heat transfer coefficient. It is found that these procedures do not introduce large errors when the flow efficiency is high, but can introduce errors as high as 100% at low flow efficiencies. Surprisingly this study shows that for large fin pitch ratios, better experimental approximations to the heat transfer coefficient are obtained when single louvers instead of a row (or fin) provide the active heat transfer surface.

Acknowledgements

Dr. Zhang was partly supported by the Air Conditioning and Refrigeration Center, Department of Mechanical and Industrial Engineering, University of Illinois, Urbana Champaign. Supercomputing time was granted by the NSF PACI program through the National Resource Allocation Committee (NRAC).

References

[1] F.N. Beauvais, An aerodynamic look at automobile radiators, SAE Paper No. 65070, 1965.

[2] C.J. Davenport, Heat transfer and flow friction characteristics of louvered heat exchanger surfaces, in: J. Taborek, G.F. Hewitt, N. Afgan (Eds.), Heat Exchangers: Theory and Practice, Hemisphere, Washington, DC, 1983, pp. 397–412.

[3] R.L. Webb, P. Trauger, Flow structure in the louvered fin heat exchanger geometry, Exp. Thermal Fluid Sci. 4 (1991) 205–217.

[4] A. Achaichia, T.A. Cowell, A finite difference analysis of fully developed periodic laminar flow in inclined louvered arrays, in: Proceedings of the Second UK National Heat Transfer Conference, Glasgow, vol. 2, 1988, pp. 883–888.

[5] K.D. Bellows, Flow visualization of louvered-fin heat exchangers, M.S. Thesis, Department of Mechanical and Industrial Engineering, University of Illinois at Urbana Champaign, 1996.

[6] L.W. Zhang, D.K. Tafti, F.M. Najjar, S. Balachandar, Computations of flow and heat transfer in parallel-plate fin heat exchangers on the CM-5: effects of flow unsteadiness and three-dimensionality, Int. J. Heat Mass Transfer 40 (1997) 1325–1341.

[7] L.W. Zhang, S. Balachandar, D.K. Tafti, F.M. Najjar, Heat transfer enhancement mechanisms in inline and staggered parallel-plate fin heat exchangers, Int. J. Heat Mass Transfer 40 (10) (1997) 2307–2325.

[8] D.K. Tafti, L.W. Zhang, G. Wang, Time-dependent calculation procedure for fully developed and developing flow and heat transfer in louvered fin geometries, Numer. Heat Transfer, Part A 35 (1999) 225–249.

[9] D.K. Tafti, G. Wang, W. Lin, Flow transition in a multilouvered fin array, Int. J. Heat Mass Transfer 43 (2000) 901–919.

[10] D.K. Tafti, X. Zhang, W. Huang, G. Wang, Large-eddy simulations of flow and heat transfer in complex three-dimensional multilouvered fins, by invitation, in: Proceedings of the 2000 ASME Fluids Engineering Division Summer Meeting, 11–15 June 2000, paper no. FEDSM2000-11325, Boston, MA.

[11] K. Suga, H. Aoki, Numerical study on heat transfer and pressure drop in multilouvered fins, ASME/JSME Thermal Eng. Proc. 4 (1991) 361–368.

[12] H.C. Kang, M.H. Kim, Effect of strip location on the air-side pressure drop and heat transfer in strip fin- and tube heat exchanger, Int. J. Refrigeration 22 (1999) 302–312.

[13] J.P. Rugh, J.T. Pearson, S. Ramadhyani, A study of a very compact heat exchanger used for passenger compartment heating in automobiles, HTD-vol 201, Compact Heat Exchangers for Power and Process Industries, ASME, 1992.

[14] R.L. Webb, S.-H. Jung, Air-side performance of enhanced brazed aluminum heat exchangers, ASHRAE Transactions: Symposia, BA-92-4-2.

[15] H. Zhang, X. Lang, The experimental investigation of oblique angles and interrupted plate lengths for louvered fins in compact heat exchangers, Exp. Thermal Fluid Sci. 2 (1989) 100–106.

[16] H. Aoki, T. Shinagawa, K. Suga, An experimental study of the local heat transfer characteristics in automotive louvered fins, Exp. Thermal Fluid Sci. 2 (1989) 293–300.